JACS
JOURNAL OF THE AMERICAN CHEMICAL SOCIETY
pubs.acs.org/JACS
Article

Just Add Water: Modulating the Structure-Derived Acidity of Catalytic Hexameric Resorcinarene Capsules

David A. Poole, III, Simon Mathew, and Joost N. H. Reek*

Cite This: J. Am. Chem. Soc. 2021, 143, 16419−16427
Read Online
ACCESS | Metrics & More | Article Recommendations | Supporting Information

ABSTRACT: The hexameric undecyl-resorcin[4]arene capsule ($^{C11}\mathbf{R}_6$) features eight discrete structural water molecules located at the vertices of its cubic suprastructure. Combining NMR spectroscopy with classical molecular dynamics (MD), we identified and characterized two distinct species of this capsule, $^{C11}\mathbf{R}_6$-**A** and $^{C11}\mathbf{R}_6$-**B**, respectively featuring 8 and 15 water molecules incorporated into their respective hydrogen-bonded networks. Furthermore, we found that the ratio of the $^{C11}\mathbf{R}_6$-**A** and $^{C11}\mathbf{R}_6$-**B** found in solution can be modulated by controlling the water content of the sample. The importance of this supramolecular modulation in $^{C11}\mathbf{R}_6$ capsules is highlighted by its ability to perform acid-catalyzed transformations, which is an emergent property arising from the hydrogen bonding within the suprastructure. We show that the conversion of $^{C11}\mathbf{R}_6$-**A** to $^{C11}\mathbf{R}_6$-**B** enhances the catalytic rate of a model Diels−Alder cyclization by 10-fold, demonstrating the cofactor-derived control of a supramolecular catalytic process that emulates natural enzymatic systems.

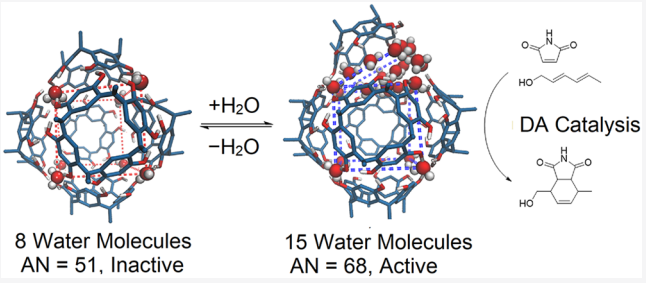

INTRODUCTION

Supramolecular catalysis derives inspiration from enzymes, translating natural features into synthetic systems to attain higher levels of control in chemical processes. Approaches toward bioinspired supramolecular catalysis include the biomimicry,[1−4] second coordination sphere design,[5−7] and confinement of the catalytic site.[8−14]

Along these lines, the positioning of catalytic active sites within well-defined capsules has been demonstrated to enable the control of catalyst properties to promote selective catalytic transformations.[6,7] In natural systems, enzymatic activity that enables the self-steering of catalytic processes necessary for metabolism can be modulated via allosteric modifications by physiochemical inputs. Although it is an intrinsic feature of natural systems, analogous modulation of catalyst properties in synthetic mimics are rare.[15−18]

It is now more than 30 years ago that the Aoyama group described the host−guest chemistry of resorcin[4]arenes in nonpolar organic solvents.[19−22] As further characterization developed, the hexameric nature of these capsules was realized and its capacity for host−guest interactions were extensively characterized.[23−38] Analogous to an enzyme, $^{C11}\mathbf{R}_6$ exhibits catalytic function from the elevated Brønsted acidity emerging from its supramolecular structure.[39] Illustrated in Figure 1, this capsule is formed in nonpolar solvents (e.g., chloroform) through the self-assembly of six facial monomers in a cubic arrangement, featuring eight water molecules (one per vertex).[23] The edges of $^{C11}\mathbf{R}_6$ are held together by hydrogen-bond network edges between adjacent facial monomers, with each end point capped at the vertex with a water molecule, completing the cubic structure.[23]

The hydrogen-bond network of $^{C11}\mathbf{R}_6$ results in the enhanced Brønsted acidity beyond that of the individual monomer units.[39] This feature has driven the application of $^{C11}\mathbf{R}_6$ as a supramolecular, organic Brønsted acid catalyst for chemical transformations under mild conditions.[40−43] In addition, the hydrogen-bond rich environment of the internal cavity within $^{C11}\mathbf{R}_6$ has been utilized as a supramolecular organocatalyst,[44−51] demonstrating a host-selective reactivity based on substrate size, and substrate−bond activation via supramolecular interactions. The use of a supplemental protic acid cocatalyst (typically HCl) extends the scope of $^{C11}\mathbf{R}_6$ activity,[52−63] notably for application toward facile synthesis of high-value terpene derivatives.[59−63] Further reactivity has been demonstrated in host-catalyzed Diels−Alder cyclization.[64]

Beyond the intrinsic Brønsted acidity of $^{C11}\mathbf{R}_6$, this supramolecule possesses an internal cavity (ca. 1400 Å^3),[23] permitting the encapsulation of transition metal catalysts[65−68] or organic catalysts[69−71] within its cavity. In these instances, the internal surface of the capsule serves as a second coordination-sphere to modulate or enhance catalytic function.[5−7]

Received: May 12, 2021
Published: September 30, 2021

https://doi.org/10.1021/jacs.1c04924
J. Am. Chem. Soc. 2021, 143, 16419−16427

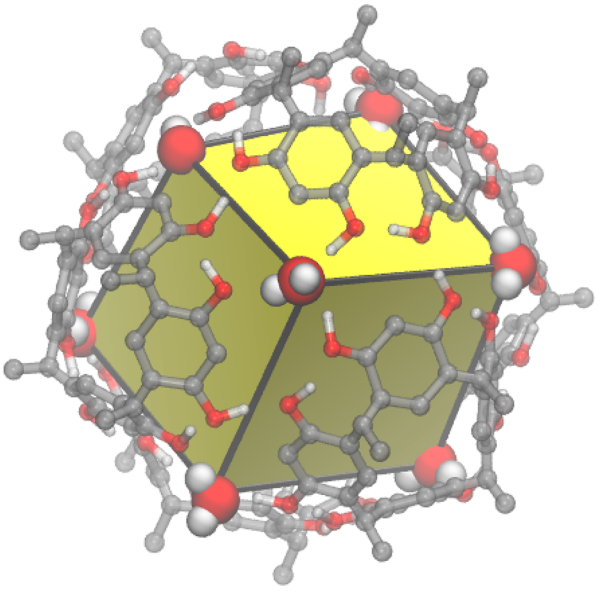

Figure 1. Ball-and-stick rendering of a model $^{C11}\mathbf{R}_6$ showing a cubic structure with 6 resorcin[4]arenes (CPK rendering) forming the faces of the cube (yellow) held together by an hydrogen-bond network continuous along each edge (black line), and capped by eight water molecules at the vertex positions (van der Waals volume renderings). To improve clarity, pendant alkyl groups and nonhydroxy hydrogen atoms were omitted from this figure.

Both the acidity and host-capacity of $^{C11}\mathbf{R}_6$ are derived from its structure.[23,39] Recent work by Payne and Oliver have demonstrated structural modification of $^{C11}\mathbf{R}_6$ by the incorporation of alcoholic solvent molecules into the hydrogen bond network,[72] complementing previous studies by Cohen[73−75] and Schnatwinkel,[76] which featured similar inclusion of long chain alcohols into the hydrogen-bond network. Interestingly, Katiyar has reported the association of free water to the capsule's hydrogen-bond network,[77,78] beyond the 8 molecules needed for capsule assembly.[23,31,32] Studies by Merget suggest that the presence of additional water may impact the catalytic activity of the $^{C11}\mathbf{R}_6$ capsule in acid-promoted cyclization of terpenes.[60] Together these findings suggest that polar molecules such as water may act as cofactors able to modulate the structure and acidity of $^{C11}\mathbf{R}_6$, analogous to the allosteric control of enzymes (e.g., cytochrome p450 oxidases, nitric oxide synthases, etc.). Understanding that these structural changes would provide insights into the previously observed water-dependent catalytic behavior and fine control the capsule's catalytic activity.

In this work, we investigate the structural changes of $^{C11}\mathbf{R}_6$ capsules through classical molecular dynamics (MD) simulations, which is further supported by ^{1}H NMR spectroscopy. Using MD, we find that $^{C11}\mathbf{R}_6$ interconverts between two assemblies as summarized by Figure 2. The $^{C11}\mathbf{R}_6$-**A** assembly features 8 water molecules at the vertex positions—in line with previous reports of $^{C11}\mathbf{R}_6$ structure[23]—while $^{C11}\mathbf{R}_6$-**B** has 14−15 water molecules, 6−7 of which spontaneously incorporate into a single edge of the cubic suprastructures, referred to here as "incorporated water" (Scheme 1). This computational finding is supported by NMR studies of water association, revealing a water-dependent equilibrium between the two capsule species differing significantly in their hydrogen-bond network. Differences between the $^{C11}\mathbf{R}_6$-**A** and $^{C11}\mathbf{R}_6$-**B** assemblies are substantiated by ^{31}P NMR chemical shifts of an encapsulated phosphine oxide, revealing different internal acidities quantified

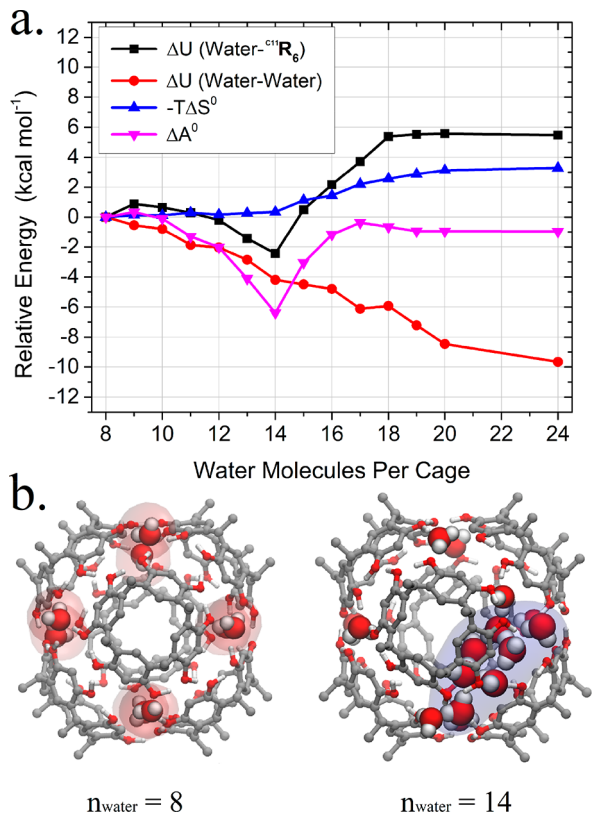

Figure 2. (a) Plot of the relative Helmholtz free energies (ΔA), internal energy (ΔU) of the water−water or water−$^{C11}\mathbf{R}_6$ interactions, and entropy (ΔS) for the incorporation of water molecules beyond 8 determined by the GIST method.[79] (b) Renderings depicting the structures of $^{C11}\mathbf{R}_6$-**A** and $^{C11}\mathbf{R}_6$-**B** containing 8 and 14 water molecules, respectively. Renderings feature highlights indicating structural (red) and incorporated (blue) water, which differentiate ^{C11}**R6-A** and $^{C11}\mathbf{R}_6$-**B**, respectively. Note that structural water highlights for $^{C11}\mathbf{R}_6$-**B** are omitted for clarity. Similarly, alkyl pendant groups, solvent, and nonhydroxy hydrogen atoms are omitted from both renderings for clarity. Both thermodynamic calculations (a) and model visualizations (b) were generated from 28 800 ns MD trajectories.

Scheme 1. Simplified Representation of the Water-Dependent Conversion between the Two Forms of $^{C11}\mathbf{R}_6$, Highlighting the 8 Water Molecules Necessary for Capsule Formation (Red) and the 7 Additional Water Molecules (Cyan) That Effect the Transition by Association to a Capsule Edge (Black Line)

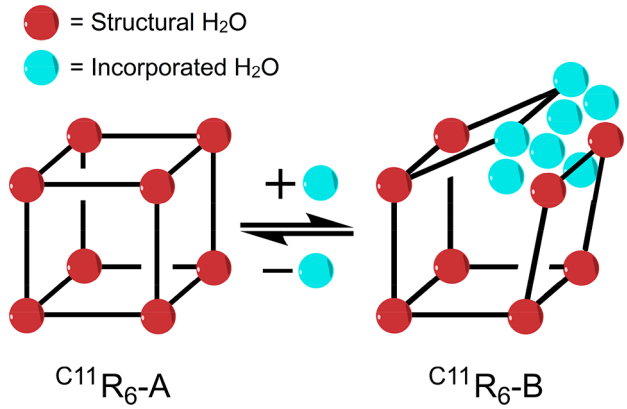

https://doi.org/10.1021/jacs.1c04924
J. Am. Chem. Soc. 2021, 143, 16419−16427

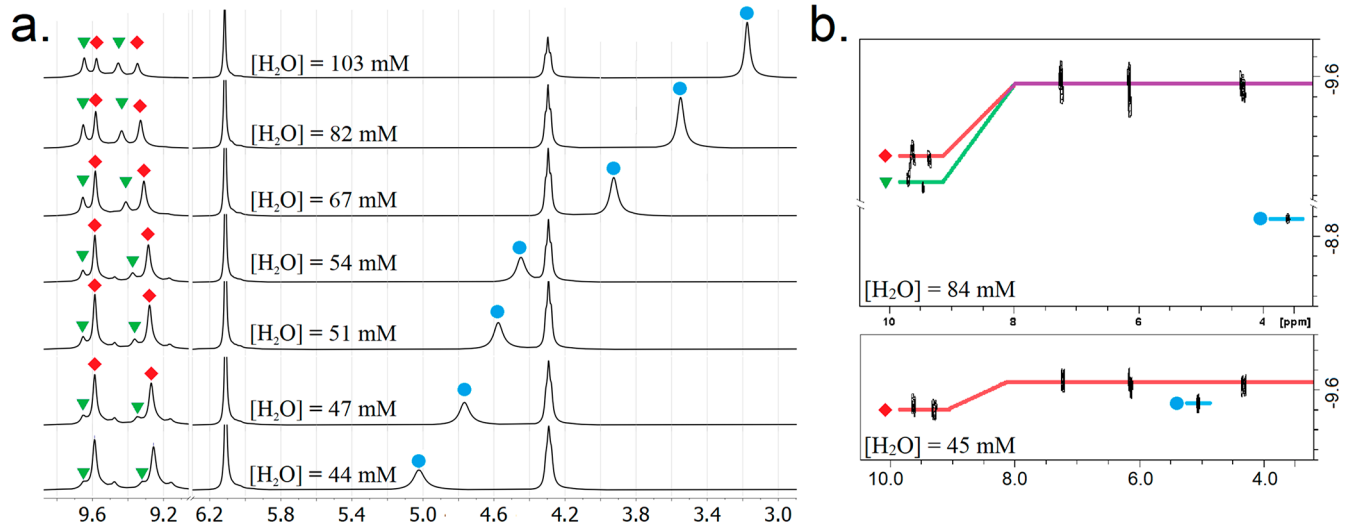

Figure 3. Quantitative ^{1}H NMR spectra (a) and DOSY diffusograms (b) of $^{C11}\mathbf{R}_6$ (5.38 mM) observed over a range of water concentrations (44.12−103.01 mM) corresponding to 8−19 water molecules per $^{C11}\mathbf{R}_6$ capsule. Water peaks and diffusion traces are highlighted in blue or accompanied by a blue circle. Peaks and diffusion traces attributed to $^{C11}\mathbf{R}_6$-**A** (red highlight and diamond) and $^{C11}\mathbf{R}_6$-**B** (green highlight and triangle) assemblies are annotated. Overlapping diffusion traces are shown in purple. Quantitation of water concentration was determined by integration of the water peak (blue circle) compared to a peak corresponding to both $^{C11}\mathbf{R}_6$ assemblies (δ = 6.2 ppm, 24 H, 5.38 mM). Complete diffusograms are provided in the Supporting Information (Figure S4). Long recycle delays (25 s) were necessary to obtain quantitative spectra for both water (T_1 = 0.7−0.9 s, data not shown) and $^{C11}\mathbf{R}_6$ (T_1 = 1.39 s, data not shown).

by their Guttman−Beckett acceptor number (AN). This difference in internal acidity allows the rate modulation of $^{C11}\mathbf{R}_6$ catalyzed Diels−Alder cycloaddition of maleimide and sorbic alcohol, demonstrating novel control of an abiotic homogeneous catalytic process.

RESULTS AND DISCUSSION

MD Simulations Reveal Distinct Species. Simulations containing explicitly solvated $^{C11}\mathbf{R}_6$ with a total of 8−24 explicit water molecules were propagated as molecular dynamics trajectories for a total of 10 μs using optimized force field parameters (Figure S1). Unfortunately, simulations featuring randomly placed water molecules and undecyl-resorcin[4]arene monomers ($^{C11}\mathbf{R}_1$) failed to self-assemble over several μs of MD propagation (results not reported). Therefore, we found it necessary to include the 8 structural water molecules, placed at the vertex positions of the capsule, while the remaining water molecules were positioned randomly in the periphery of the capsule.

In simulations containing 8−12 water molecules, we observe the external attachment of free water to the $^{C11}\mathbf{R}_6$ in line with previous reports.[77,78] Simulations containing ≥14 water molecules reveal 6 additional incorporated water molecules along a single edge of the hydrogen-bond network of the $^{C11}\mathbf{R}_6$ capsule (Scheme 1), as depicted in Figure 2b. Although these incorporated water molecules are highly organized and an integral part of the hydrogen bond network (Figure S16), single water molecules still exchange rapidly with water molecules from the bulk solvent and the 8 structural waters needed to form the capsule. The mobility of the incorporated water is highlighted by the concerted migration between the hydrogen bond edges of the capsule. This migration phenomenon was qualitatively observed as a rare event in our MD simulations (Figure S15), but occur at a sub-microsecond time scale.

The incorporation of additional water into the edge of the hydrogen bond network results in a breakage of the hydrogen bond between adjacent $^{C11}\mathbf{R}_1$ faces, altering the connectivity of the supramolecular system. This change in connectivity and composition distinguishes $^{C11}\mathbf{R}_6$-**B** from the typical $^{C11}\mathbf{R}_6$-**A** assembly. Analysis of hydrogen-bonding in our MD trajectories (Figure S2) reveal a minimum of 6 extra incorporated water molecules are required to form $^{C11}\mathbf{R}_6$-**B**.

Energetic analysis of the MD data using GIST (Figure 2a) distinguishes between both attached water[77,78] and the incorporated water we observe in $^{C11}\mathbf{R}_6$-**B**. While GIST does not provide complete free energy differences between $^{C11}\mathbf{R}_6$-**A** and $^{C11}\mathbf{R}_6$-**B**, it is useful in the analysis of favorable water structures found in our MD simulations. In simulations containing 8−12 water molecules the attached water is observed. Interestingly, the GIST-determined ΔA is similar to previously reported values (ca. −2.0 kcal mol^{-1}),[77,78] and from our analysis this is driven entirely by a favorable water−water interaction (Figure 2a, $\Delta U_{\text{water-water}}$). The inclusion of water along the hydrogen bond edge is optimal in the presence of 14 water molecules, where an additional favorable water-capsule interaction (Figure 2a, $\Delta U_{\text{water-C11R6}}$), resulting in a very favorable association (ΔA = −6.3 kcal mol^{-1}). While the incorporation of further water molecules within the supra-structure is possible, it incurs an increasing penalty from internal energy (Figure 2a, ΔU) and system entropy (Figure 2a, $-T\Delta S$). The specificity of $^{C11}\mathbf{R}_6$-**B** to incorporate 6 water molecules is a "goldilocks" number, originating from the required size of the hydrogen-bond network needed to fill a capsule edge (Figure 2b), resulting in favorable internal energy (Figure 2a). These "incorporated water" molecules are more mobile than their "structural water" counterparts, and are not as strongly localized. These simulations suggest that $^{C11}\mathbf{R}_6$ is found in only two forms—$^{C11}\mathbf{R}_6$-**A** containing 8 water molecules and $^{C11}\mathbf{R}_6$-**B** containing 14 water molecules—and the ratio between the two may depend on water content.

^{1}H NMR Identification of $^{C11}\mathbf{R}_6$-A and $^{C11}\mathbf{R}_6$-B. The formation of $^{C11}\mathbf{R}_6$-**A** and $^{C11}\mathbf{R}_6$-**B** was investigated by ^{1}H NMR, by measuring spectra of $^{C11}\mathbf{R}_6$ solution at various concentrations of water (44.12−103.01 mM; for details see Supporting

https://doi.org/10.1021/jacs.1c04924
J. Am. Chem. Soc. 2021, 143, 16419−16427

Information). Contrasting previous reports, which broadly attribute all phenolic peaks (δ = 8.5−10.0 ppm) to a singular species of $^{C11}\mathbf{R}_6$,[13−16] our spectra, shown in Figure 3a, reveal a changing pattern in the phenolic peaks, concomitant with the changing water content. The separation of these phenolic peaks indicates slowly exchanging environments,[80] inconsistent with the 5 ns lifetimes of previously described water dynamics.[78] As these peaks increase (or decrease) in a correlated fashion, we attribute these spectral features to distinct assemblies: $^{C11}\mathbf{R}_6$-**A** (δ = 9.58 and 9.35 ppm) and $^{C11}\mathbf{R}_6$-**B** (δ = 9.65 and 9.46 ppm). This peak assignment is further supported by inversion-relaxation measurements (Figure S21), from which identical T_1 relaxation times were obtained for the phenolic peaks of either capsule indicative of a shared environment. The increased sensitivity of T_1 relaxation times of the peaks belonging $^{C11}\mathbf{R}_6$-**B** to changing water content is in line with the larger number of water molecules associate to its structure.

Interestingly, the relative concentrations of these species vary with water content from 44.12 mM (ca. 8 water molecules per capsule) to 103.01 mM (ca. 19 water molecules per capsule). As these differences are only apparent in the phenolic region of the NMR spectrum, we surmise that these assemblies are distinguished by the structure of their respective hydrogen-bond networks. Therefore, we putatively assigned these peaks to $^{C11}\mathbf{R}_6$-**A** (δ_{OH} = 9.58, 9.35 ppm) and $^{C11}\mathbf{R}_6$-**B** (δ_{OH} = 9.65, 9.46 ppm) based on the increasing concentration of water and consistent with the structures observed in MD simulations (Figure 2). The presence of incorporated water in $^{C11}\mathbf{R}_6$-**B** is further evidenced by stronger NOE correlations between its phenolic peaks and free water (Figure S18). Deuterium exchange of the OH-groups with D_2O (Figure S23) is different for the two capsules, and evidence the discontinuous hydrogen bond network in line with our MD simulations (Figure S16).

Interestingly, only two peaks of equal area are observed for the phenolic protons of either assembly, despite the asymmetry derived by incorporated water molecules in $^{C11}\mathbf{R}_6$-**B** (Figure 2). Our MD simulations show the specific arrangement of incorporated water shift between edges of the capsule on a sub-microsecond time scale (Figure S15). The environments of the phenolic protons of $^{C11}\mathbf{R}_6$-**B**, exchange at this rate, and as such are observed as a time-averaging signal. Exchange of water between $^{C11}\mathbf{R}_6$-**B** and $^{C11}\mathbf{R}_6$-**A** is relatively slow leading to distinct phenolic peaks that can be distinguished in the NMR spectra (Figure S14).[80] On the basis of the relative strength of NOE correlations between the phenolic peaks and water, we assign the upfield peaks of either assembly (δ = 9.35 and 9.46 ppm) to the 24 phenolic protons adjacent to the structural water sites (Figure 1). Similarly the downfield peaks of either assembly (δ = 9.58 and 9.65 ppm), are assigned to the remaining 24 phenolic protons which participate in hydrogen bonding between and within the resorcin[4]arene monomer faces. Fortunately, the separation of the pairs (33 Hz) of the resolved $^{C11}\mathbf{R}_6$-**A** and $^{C11}\mathbf{R}_6$-**B** phenolic peaks constraints the rate constant for chemical exchange (k_{ex}) between the two assemblies to <155 s^{-1} (for a detailed discussion see, Figure S14).[80]

The apparent diffusion of these phenolic peaks appears faster than the other peaks (Figure 3b) due to proton exchange with water occurring within the diffusion time in the measurement (Δ = 100 ms). Fortunately, the pairing of these diffusion traces further supports the speciation of the two assemblies observed by the correlation of the peak areas (Figure 3a).

Further characterization of the capsule using ^{1}H NMR (Figure S3), DOSY (Figures 3b and S4),[31−33,77] and solution state FTIR (Figure S5)[36] indicate that both assemblies are hexameric assemblies with a similar Stokes radius (16.6 Å) at [H_2O] = 44 and 103 mM consistent with previous reports of $^{C11}\mathbf{R}_6$ capsule structure.[23−38]

The single observed peak of water (Figure 3) indicates that it is in a state of fast exchange between a free state in the bulk solution and a bound state, incorporated into the $^{C11}\mathbf{R}_6$ capsule (Figure S14).[82] As previous reports detail, the available water is completely incorporated into the cage at low (i.e., 44 mM) water concentrations;[31−33,77] therefore, the measured chemical shift (δ = 5.1 ppm) can be attributed to the structural water (Figure 1), as opposed to the free H_2O water-saturated chloroform.[81] As the observed chemical shift is time-averaged,[80] the proportion and quantity of water associated with $^{C11}\mathbf{R}_6$ (B_{wat}) was determined directly from ^{1}H NMR spectra (Figure 3a).

Figure 4 shows the total number of water molecules associated with $^{C11}\mathbf{R}_6$ increases linearly with the proportion of $^{C11}\mathbf{R}_6$-**B** (θ_B) in the sample, with the slope showing an additional 7.27 ± 0.26 water molecules are incorporated per $^{C11}\mathbf{R}_6$-**B** formed. Thus, combined with the 8 structural waters native to $^{C11}\mathbf{R}_6$, a total of 15 water molecules are associated with $^{C11}\mathbf{R}_6$-**B**. From our MD simulations (Figure 1) we surmise that these additional water molecules are incorporated into the hydrogen bonding network of the capsule. This number is in agreement with MD models (Figure 2) that predict a minimum of 14 water molecules for the formation of $^{C11}\mathbf{R}_6$-**B** (Figure 2). The water-dependent conversion between $^{C11}\mathbf{R}_6$-**A** and $^{C11}\mathbf{R}_6$-**B** was fit using an empirical model (Figure S13) to enable estimation of the proportion of $^{C11}\mathbf{R}_6$-**B** capsules (θ_B) via water content.

^{31}P NMR Investigation of Structure-Dependent Acidity. Many catalytic applications of $^{C11}\mathbf{R}_6$ rely on the intrinsic acidity derived from its supramolecular structure.[39] The 33 Hz downfield shift of the $^{C11}\mathbf{R}_6$-**B** phenolic protons (Figure 3a) suggest an increased acidity (compared to $^{C11}\mathbf{R}_6$-**A**),[82] a feature which is further supported by their apparent diffusivities observed by DOSY (Figure 3b).

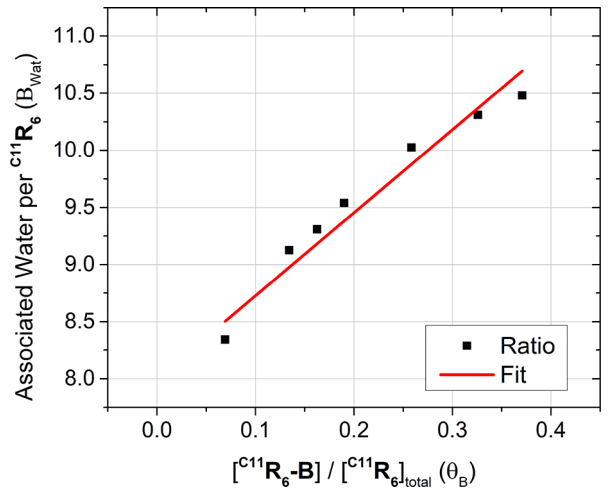

Figure 4. Plot of the total number of associated waters (B_{wat}) and proportion of $^{C11}\mathbf{R}_6$-**B** capsules (θ_B) determined from ^{1}H NMR measurements (Figure 3a). The association of an additional 7.27 ± 0.26 water molecules concomitant to conversion is determined from the slope of the linear fit (red).

https://doi.org/10.1021/jacs.1c04924
J. Am. Chem. Soc. 2021, 143, 16419−16427

Previously the Brønsted acidity of $^{C11}\mathbf{R_6}$ assemblies were measured using nitrogen bases to estimate aqueous-equivalent pK_a values.[39] Unfortunately, this protocol impairs the accurate determination of water content by either Karl–Fischer titration or ^{1}H NMR integration, and could not be used to differentiate the acidity of $^{C11}\mathbf{R_6}$-**A** and $^{C11}\mathbf{R_6}$-**B**.

Therefore, we investigate the ability of structure-dependent acidity to modulate the interaction strength with tri-*n*-butyl phosphine oxide (Bu_3PO) as guest through ^{31}P NMR (Figure 5).[83,84] The encapsulation of Bu_3PO was readily confirmed by ^{1}H NMR, showing the development of broad upfield peaks (δ = −2.0–0.5 ppm), typically observed for encapsulated guests.[24−38] The binding of Bu_3PO within the capsule was further evidenced by ^{1}H DOSY measurements (Figure S12), with similar diffusion for the $^{C11}\mathbf{R_6}$ host and upfield peaks (log D = −9.0, see Figure 3b).

A downfield chemical shift in ^{31}P NMR is expected when a Bu_3PO forms a hydrogen-bond adduct with another species, such as when encapsulated within $^{C11}\mathbf{R_6}$ and the degree of this shift is proportionate to the acidity of the hydrogen-bond donor.[83,84] Three peaks ($^{31P}\delta \approx$ 55.0–65.0 ppm) were consistently observed in the ^{31}P NMR spectra of the encapsulated Bu_3PO (Figures S9 and S10). The upfield peak ($^{31P}\delta \approx$ 55.0–64.0 ppm) was assigned to the free Bu_3PO by observed correlations to the protons of the free species by ^{1}H–^{31}P HMBC (Figure S11). A low intensity peak ($^{31P}\delta \approx$ 64.0–65.0 ppm) was observed in all spectra, with a low intensity that waned with increasing water content. This spectral feature is particularly evident at a minimal water concentration (44.18 mM water, Figure S8), where the majority of the Bu_3PO (3.50 mM) was observed to be encapsulated. Unfortunately, two-dimensional techniques (e.g., HMBC) could not provide sufficient cross-peaks with which to identify the originating species by other means. With additional water this minor peak broadens and diverges compared to the major peaks, and we infer that exchange between this minor species and the observed major peak is unlikely based on the diverging chemical shift. On the basis of the low intensity of the ^{31}P signal, we surmise that this spectral feature does not correspond to the free or encapsulated Bu_3PO, and its identity is unlikely to interfere with measurements of the $^{C11}\mathbf{R_6}$ capsule's internal acidity. The remaining peak was attributed to the $^{C11}\mathbf{R_6}$-associated Bu_3PO ($^{31P}\delta \approx$ 60.0–64 ppm) based on its apparent intensity (Figures S9 and S10). All three peaks were observed to move in a concerted fashion with changes in water content, which we ascribe to changes in bulk dielectric of the solvent medium.[85]

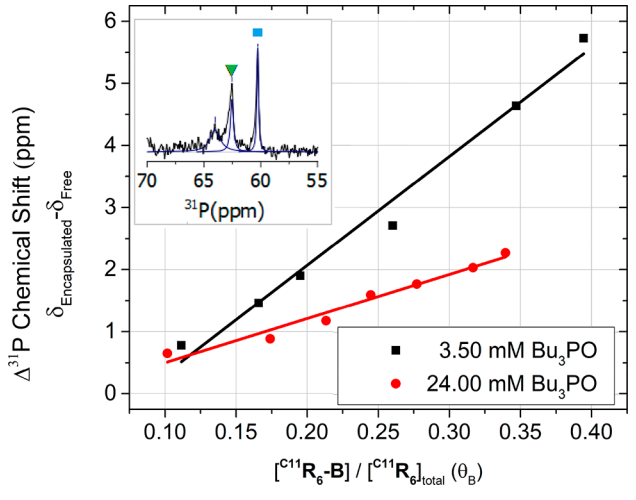

Figure 5. Chemical shift difference between free and encapsulated Bu_3PO observed by ^{31}P NMR at two concentrations, 3.50 mM (black) and 24.00 mM (red) in the presence of $^{C11}\mathbf{R_6}$ (5.38 mM). Spectra were obtained at water contents spanning 43.76–110.19 mM (3.50 mM Bu_3PO) and 43.05–86.53 mM (24.00 mM Bu_3PO), which were subsequently converted to the proportion of $^{C11}\mathbf{R_6}$-**B** (θ_B) by an empirical model (Figure S13). Inset, a ^{31}P NMR spectrum showing peaks corresponding to encapsulated (▼, green) and free (■, blue) Bu_3PO.

The free and encapsulated Bu_3PO afford distinct peaks in slow exchange (Figure 5, inset). Similar to observations made with ^{1}H NMR (Figure 3), differentiation between phosphine oxide encapsulated within $^{C11}\mathbf{R_6}$-**A** and $^{C11}\mathbf{R_6}$-**B** was not observed by ^{31}P due to the similarities of the magnetic environments experienced by the phosphorus nuclei. Due to this similarity, the shift of the observable peak corresponds to the time weighted average of the Bu_3PO encapsulated within $^{C11}\mathbf{R_6}$-**A** and $^{C11}\mathbf{R_6}$-**B** (see Figure S14a for an example of the exchange of indistinguishable nuclei).[80] Further complications arise as a phosphine oxide guest within $^{C11}\mathbf{R_6}$-**A** or $^{C11}\mathbf{R_6}$-**B** may exchange hydrogen bonding partners within the capsule at a time scale faster than NMR measurement,[80] resulting in a single observable peak with a shift that is the time weighted average of the hydrogen bonding states (see Figure S14b for a detailed example of the exchange of a rapid process). The result of these exchange processes is a single observable peak corresponding to Bu_3PO encapsulated by $^{C11}\mathbf{R_6}$-**A** or $^{C11}\mathbf{R_6}$-**B**, in all states of hydrogen bonding (see Figure S14 for a detailed explanation).[80]

Despite these limits in observation, the strength of the interaction between $^{C11}\mathbf{R_6}$ and Bu_3PO can be correlated to the downfield chemical shift of the single observable peak ($^{31P}\delta$ = 64.0–60.0 ppm). The strength of the interaction between Bu_3PO and $^{C11}\mathbf{R_6}$ can be determined by modulating the Brønsted acidity through changing the content of the sample (i.e., varying the water content of the sample) as shown in Figure 5. Two sets of experiments were performed where the $^{C11}\mathbf{R_6}$-**A**/$^{C11}\mathbf{R_6}$-**B** ratio was modulated through controlling water content (44.18–110.19 mM and 43.05–86.53 mM, respectively) in the presence of either a low (3.50 mM) or high (24.00 mM) concentration of Bu_3PO. While the high concentration is analogous to catalytic conditions, at lower concentrations the Bu_3PO probe selectively associates to the stronger interacting (i.e., more acidic) assembly. From these contrasting measurements we determine that the environment of $^{C11}\mathbf{R_6}$-**B** is more acidic than $^{C11}\mathbf{R_6}$-**A**, which may enhance its catalytic activity. We rationalize the increased acidity of $^{C11}\mathbf{R_6}$-**B** by the increased availability of protons within the capsule from the weakly bound incorporated water molecules (Scheme 1).

Similar to 4 of the structural water molecules of $^{C11}\mathbf{R_6}$-**A**,[39] the 7 incorporated water molecules found in $^{C11}\mathbf{R_6}$-**B** are capable hydrogen-bond donors, and may also act as acids stabilized by the edge hydrogen-bond network (Figure S16).

The Guttman–Becket acceptor number (AN) is a measure of Lewis acidity that quantifies the differences in acidity between the two capsules, and allows comparison of acid catalysts in solvent media.[84] On the basis of ^{31}P NMR spectra obtained at a minimal water concentration ([H_2O] = 44.18 mM, Figure S8), we have estimated the Lewis acidity of $^{C11}\mathbf{R_6}$-**A** (AN = 51), similar to $B(OMe)_3$ (AN = 51).[84] By extrapolating the chemical shift difference observed with Bu_3PO (3.5 mM, Figure 5), we

https://doi.org/10.1021/jacs.1c04924
J. Am. Chem. Soc. 2021, 143, 16419–16427

estimate the Lewis acidity of $^{C11}\mathbf{R}_6$-**B** assemblies (AN = 68 ± 1), similar to $TiCl_4$ (AN = 70).[86]

Structural Modulation of the $^{C11}\mathbf{R}_6$-Catalyzed Diels–Alder Cycloaddition. We investigated the catalytic activity of the two $^{C11}\mathbf{R}_6$ assemblies in the Diels–Alder cycloaddition of maleimide and sorbic alcohol to produce 4-(hydroxymethyl)-7-methyl-3a,4,7,7a-tetrahydro-1*H*-isoindole-1,3(2*H*)-dione (Figure 6, inset). The Diels–Alder reaction was explicitly chosen as a probe for the structure-dependent catalytic activity of $^{C11}\mathbf{R}_6$ as it proceeds without the generation of water or acid as a byproduct. Specifically, catalysis was performed at different water concentrations ([H_2O] = 8.76–25.95 mM) enabling modulation of the $^{C11}\mathbf{R}_6$-**B** proportion (θ_B = 0.12–0.44) within the mixture. The dependency of catalytic activity on the proportion of $^{C11}\mathbf{R}_6$-**B** was revealed, with the result depicted in Figure 6.

The initial reaction rates reveal that increases in water content afforded a doubling of the observed reaction rate (0.65–1.15 h^{-1}), an effect not observed in the absence of $^{C11}\mathbf{R}_6$ (Figure S7). As the ratio of $^{C11}\mathbf{R}_6$-**A** and $^{C11}\mathbf{R}_6$-**B** could not be directly observed by NMR, they were computed from the measured water content in conjunction with our empirical model (eq S1). The observed reaction velocity increases linearly (θ_B = 0.1–0.3) with the formation of $^{C11}\mathbf{R}_6$-**B** until it plateaus (θ_B = 0.3–0.5), where another process becomes rate limiting. We propose that this rate limitation is due to the slow isomerization of sorbyl alcohol from its inactive *s-trans* isomer to the active *s-cis* isomer (Figure S17). From this limitation we surmise that ^{C11}**R6** acts primarily as an acid-catalyst for the activation of maleimide. A linear fit of the reaction rate to the proportion of $^{C11}\mathbf{R}_6$-**B** (θ_B) between 0.1–0.3 decomposes the overall reaction rate to the activity of either $^{C11}\mathbf{R}_6$-**A** or $^{C11}\mathbf{R}_6$-**B** assemblies. From this linear fit we find the more acidic $^{C11}\mathbf{R}_6$-**B** (2.16 ± 0.29 h^{-1}) is significantly more active than $^{C11}\mathbf{R}_6$-**A** (0.24 ± 0.06 h^{-1}). As the computed rate of $^{C11}\mathbf{R}_6$-**A** catalyzed cycloadditions is close to the uncatalyzed reaction (0.21 ± 0.01 h^{-1}, Figure S7) we surmise that $^{C11}\mathbf{R}_6$-**B** is the sole active catalytic species. This result highlights the similarities between biological and supramolecular catalytic systems, where subtle changes in the arrangement of (supra)molecular features yield significant changes in catalytic output under mild conditions.

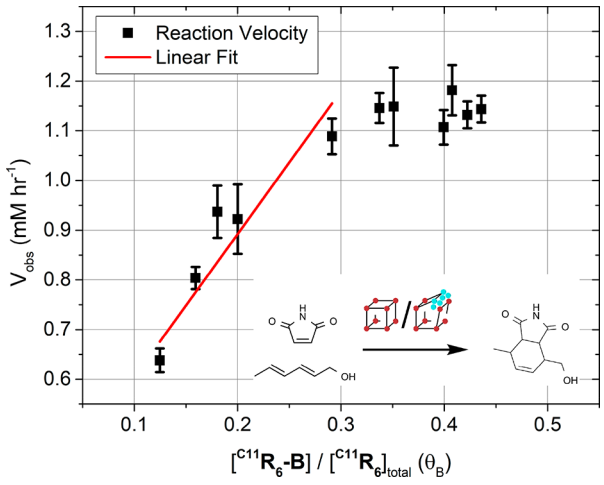

Figure 6. Initial reaction velocities, V_{obs}, for the Diels–Alder cycloaddition of sorbic alcohol (6.00 mM), and maleimide (6.00 mM), catalyzed by $^{C11}\mathbf{R}_6$ (1.34 mM, 22 mol %) in $CDCl_3$ under ambient conditions (25 °C). Reaction velocity was measured by the depletion of maleimide (δ = 6.72 ppm) referenced to a TMS standard by ^{1}H NMR. Reaction water content spanned 11.77–34.87 mM (8.76–25.95 molecules per capsule) as determined by Karl–Fischer titration. The water content was used to estimate $^{C11}\mathbf{R}_6$-**B** conversion by an empirical model (eq S1). Error bars correspond to the standard error in the linear fitting of the initial reaction velocity (Figure S6). A linear fit (red) reveals the turnover frequency of $^{C11}\mathbf{R}_6$-**A** (0.24 ± 0.06 h^{-1}) and $^{C11}\mathbf{R}_6$-**B** (2.16 ± 0.29 h^{-1}).

CONCLUSION

On the basis of NMR spectroscopy and computational data we demonstrate that the self-assembled hexameric undecylresorcin[4]arene capsule $^{C11}\mathbf{R}_6$ can be switched between two distinct species—$^{C11}\mathbf{R}_6$-**A** and $^{C11}\mathbf{R}_6$-**B**—respectively featuring 8 and 15 water molecules within their hydrogen-bond networks. The internal environments of the two assemblies were probed by the binding of Bu_3PO, revealing substantial shifts in the ^{31}P NMR peak of this guest through changing the $^{C11}\mathbf{R}_6$-**A**/$^{C11}\mathbf{R}_6$-**B** ratio by the addition of water to the sample. These NMR experiments suggest a stronger acidity of $^{C11}\mathbf{R}_6$-**B** assemblies that translate into differences in catalytic activity. The catalytic activity of these two assemblies were investigated in a Diels–Alder cycloaddition reaction, revealing that $^{C11}\mathbf{R}_6$-**B** exhibits greater catalytic output by an order of magnitude. This study demonstrates the ability of water to effect structural changes in $^{C11}\mathbf{R}_6$ capsules by modulating the structure-derived catalytic properties of the supramolecular assembly. We envisage that the present work will enable subsequent study of other small-molecules as structural effectors of $^{C11}\mathbf{R}_6$ (and related supramolecular structures) with the goal of gated and self-steering catalytic applications.

ASSOCIATED CONTENT

Supporting Information

The Supporting Information is available free of charge at https://pubs.acs.org/doi/10.1021/jacs.1c04924.

Computational simulation parameters, experimental conditions, spectral data for all measurements (PDF)

Coordinates and connectivity of a representative structure for $^{C11}\mathbf{R}_6$-**A** (PDB)

Coordinates and connectivity of a representative structure for $^{C11}\mathbf{R}_6$-**B** (PDB)

Coordinates, charge and connectivity of undecylresorcin[4]arene monomer subunit used in MD simulations (monomer.mol2); Force field parameters used for MD simulation provided in Amber format (sim.frcmod) (ZIP)

AUTHOR INFORMATION

Corresponding Author

Joost N. H. Reek – *Homogeneous, Supramolecular, and Bioinspired Catalysis Group, van't Hoff Institute for Molecular Science (HIMS), University of Amsterdam (UvA), 1098 XH Amsterdam, The Netherlands;* orcid.org/0000-0001-5024-508X; Email: j.n.h.reek@uva.nl

Authors

David A. Poole, III – *Homogeneous, Supramolecular, and Bioinspired Catalysis Group, van't Hoff Institute for Molecular Science (HIMS), University of Amsterdam (UvA), 1098 XH Amsterdam, The Netherlands*

Simon Mathew – *Homogeneous, Supramolecular, and Bioinspired Catalysis Group, van't Hoff Institute for*

Molecular Science (HIMS), University of Amsterdam (UvA), 1098 XH Amsterdam, The Netherlands; orcid.org/0000-0003-2480-3222

Complete contact information is available at: https://pubs.acs.org/10.1021/jacs.1c04924

Notes

The authors declare no competing financial interest.

■ ACKNOWLEDGMENTS

We thank our colleagues Dr. Anne Jans, Eline Meijer, and Dr. Andreas Ehlers for their assistance and advice for this study. We thank the European Research Council (ERC Adv. Grant 339786-5354 NAT_CAT) and the sustainable chemistry research program from the University of Amsterdam for financial support.

■ REFERENCES

(1) Rebilly, J.-N.; Colasson, B.; Bistri, O.; Over, D.; Reinaud, O. Biomimetic cavity-based metal complexes. *Chem. Soc. Rev.* **2015**, *44* (2), 467−489.
(2) Breslow, R.; Dong, S. D. Biomimetic Reactions Catalyzed by Cyclodextrins and Their Derivatives. *Chem. Rev.* **1998**, *98* (5), 1997−2012.
(3) Marchetti, L.; Levine, M. Biomimetic Catalysis. *ACS Catal.* **2011**, *1* (9), 1090−1118.
(4) Tu, Y.; Peng, F.; Adawy, A.; Men, Y.; Abdelmohsen, L. K. E. A.; Wilson, D. A. Mimicking the Cell: Bio-Inspired Functions of Supramolecular Assemblies. *Chem. Rev.* **2016**, *116* (4), 2023−2078.
(5) Elsby, M. R.; Baker, R. T. Strategies and mechanisms of metal−ligand cooperativity in first-row transition metal complex catalysts. *Chem. Soc. Rev.* **2020**, *49*, 8933−8987.
(6) Zhao, M.; Wang, H.-B.; Ji, L.-N.; Mao, Z.-W. Insights into metalloenzyme microenvironments: biomimetic metal complexes with a functional second coordination sphere. *Chem. Soc. Rev.* **2013**, *42* (21), 8360.
(7) Trouve, J.; Gramage-Doria, R. Beyond hydrogen bonding: recent trends of outer sphere interactions in transition metal catalysis. *Chem. Soc. Rev.* **2021**, *50*, 3565−3584.
(8) Nurttila, S. S.; Linnebank, P. R.; Krachko, T.; Reek, J. N. H. Supramolecular Approaches to Control Activity and Selectivity in Hydroformylation Catalysis. *ACS Catal.* **2018**, *8*, 3469−3488.
(9) Meeuwissen, J.; Reek, J. N. H. Supramolecular catalysis beyond enzyme mimics. *Nat. Chem.* **2010**, *2*, 615−621.
(10) Gaeta, C.; La Manna, P.; De Rosa, M.; Soriente, A.; Talotta, C.; Neri, P. Supramolecular Catalysis with Self-Assembled Capsules and Cages: What Happens in Confined Spaces. *ChemCatChem* **2021**, *13* (7), 1638−1658.
(11) Grommet, A. B.; Feller, M.; Klajn, R. Chemical reactivity under nanoconfinement. *Nat. Nanotechnol.* **2020**, *15*, 256−271.
(12) Leenders, S. H. A. M.; Gramage-Doria, R.; de Bruin, B.; Reek, J. N. H. Transition metal catalysis in confined spaces. *Chem. Soc. Rev.* **2015**, *44*, 433−448.
(13) Morimoto, M.; Bierschenk, S. M.; Xia, K. T.; Bergman, R. G.; Raymond, K. N.; Toste, F. D. Advances in supramolecular host-mediated reactivity. *Nature Catalysis* **2020**, *3*, 969−984.
(14) Yoshizawa, M.; Klosterman, J. K.; Fujita, M. Functional Molecular Flasks: New Properties and Reactions within Discrete, Self-Assembled Hosts. *Angew. Chem., Int. Ed.* **2009**, *48* (19), 3418−3438.
(15) Rieth, S.; Hermann, K.; Wang, B.-Y.; Badjic, J. D. Controlling the dynamics of molecular encapsulation and gating. *Chem. Soc. Rev.* **2011**, *40*, 1609−1622.
(16) Blanco-Gómez, A.; Cortón, P.; Barravecchia, L.; Neira, I.; Pazos, E.; Peinador, C.; García, M. Controlled binding of organic guests by stimuli-responsive macrocycles. *Chem. Soc. Rev.* **2020**, *49*, 3834−3862.
(17) Hermann, K.; Ruan, Y.; Hardin, A. M.; Hadad, C. M.; Badjić, J. D. Gated molecular baskets. *Chem. Soc. Rev.* **2015**, *44*, 500−514.
(18) Díaz-Moscoso, A.; Ballester, P. Light-responsive molecular containers. *Chem. Commun.* **2017**, *53*, 4635−4652.
(19) Aoyama, Y.; Tanaka, Y.; Sugahara, S. Molecular recognition. 5. Molecular recognition of sugars via hydrogen-bonding interaction with a synthetic polyhydroxy macrocycle. *J. Am. Chem. Soc.* **1989**, *111* (14), 5397−5404.
(20) Tanaka, Y.; Ubukata, Y.; Aoyama, Y. Selective Sugar Binding with a Synthetic Polyhydroxy Macrocycle. A Remarkable Selectivity for Fructose over Glucose. *Chem. Lett.* **1989**, *18* (11), 1905−1908.
(21) Tanaka, Y.; Kato, Y.; Aoyama, Y. Molecular recognition. Two-point hydrogen-bonding interaction: a remarkable chain-length selectivity in the binding of dicarboxylic acids with resorcinol-aldehyde cyclotetramer as a multidentate host. *J. Am. Chem. Soc.* **1990**, *112* (7), 2807−2808.
(22) Kikuchi, Y.; Tanaka, Y.; Sutarto, S.; Kobayashi, K.; Toi, H.; Aoyama, Y. Highly cooperative binding of alkyl glucopyranosides to the resorcinol cyclic tetramer due to intracomplex guest-guest hydrogen-bonding: solvophobicity/solvophilicity control by an alkyl group of the geometry, stoichiometry, stereoselectivity, and cooperativity. *J. Am. Chem. Soc.* **1992**, *114* (26), 10302−10306.
(23) MacGillivray, L. R.; Atwood, J. L. A chiral spherical molecular assembly held together by 60 hydrogen bonds. *Nature* **1997**, *389* (6650), 469−472.
(24) MacGillivray, L. R.; Atwood, J. L. Rational Design of Multicomponent Calix[4]arenes and Control of Their Alignment in the Solid State. *J. Am. Chem. Soc.* **1997**, *119* (29), 6931−6932.
(25) Cohen, Y.; Avram, L.; Frish, L. Diffusion NMR Spectroscopy in Supramolecular and Combinatorial Chemistry: An Old Parameter—New Insights. *Angew. Chem., Int. Ed.* **2005**, *44* (4), 520−554.
(26) Avram, L.; Cohen, Y. Spontaneous Formation of Hexameric Resorcinarene Capsule in Chloroform Solution as Detected by Diffusion NMR. *J. Am. Chem. Soc.* **2002**, *124* (51), 15148−15149.
(27) Avram, L.; Cohen, Y. Effect of a Cationic Guest on the Characteristics of the Molecular Capsule of Resorcinarene: A Diffusion NMR Study. *Org. Lett.* **2003**, *5* (7), 1099−1102.
(28) Avram, L.; Cohen, Y. Discrimination of Guests Encapsulation in Large Hexameric Molecular Capsules in Solution: Pyrogallol[4]arene versus Resorcin[4]arene Capsules. *J. Am. Chem. Soc.* **2003**, *125* (52), 16180−16181.
(29) Avram, L.; Cohen, Y. Hexameric Capsules of Lipophilic Pyrogallolarene and Resorcinarene in Solutions as Probed by Diffusion NMR: One Hydroxyl Makes the Difference. *Org. Lett.* **2003**, *5* (18), 3329−3332.
(30) Avram, L.; Cohen, Y. Self-Recognition, Structure, Stability, and Guest Affinity of Pyrogallol[4]arene and Resorcin[4]arene Capsules in Solution. *J. Am. Chem. Soc.* **2004**, *126* (37), 11556−11563.
(31) Avram, L.; Cohen, Y.; Rebek, J., Jr. Recent advances in hydrogen-bonded hexameric encapsulation complexes. *Chem. Commun.* **2011**, *47* (19), 5368−5375.
(32) Avram, L.; Cohen, Y. Diffusion NMR of molecular cages and capsules. *Chem. Soc. Rev.* **2015**, *44*, 586−602.
(33) Evan-Salem, T.; Baruch, I.; Avram, L.; Cohen, Y.; Palmer, L. C.; Rebek, J. Resorcinarenes are hexameric capsules in solution. *Proc. Natl. Acad. Sci. U. S. A.* **2006**, *103* (33), 12296−12300.
(34) Shivanyuk, A.; Friese, J. C.; Döring, S.; Rebek, J., Jr. Solvent-Stabilized Molecular Capsules. *J. Org. Chem.* **2003**, *68* (17), 6489−6496.
(35) Shivanyuk, A.; Rebek, J. Reversible encapsulation by self-assembling resorcinarene subunits. *Proc. Natl. Acad. Sci. U. S. A.* **2001**, *98* (14), 7662−7665.
(36) Stirling, C. J. M.; Fundin, L. J.; Williams, N. H. Trimorphism in solid resorcinarenes. *Chem. Commun.* **2007**, 1748−1750.
(37) Palmer, L. C.; Shivanyuk, A.; Yamanaka, M.; Rebek, J., Jr. Resorcinarene assemblies as synthetic receptors. *Chem. Commun.* **2005**, No. 7, 857.

(38) Atwood, J. L.; Barbour, L. J.; Jerga, A. Organization of the interior of molecular capsules by hydrogen bonding. *Proc. Natl. Acad. Sci. U. S. A.* **2002**, *99* (8), 4837−4841.
(39) Zhang, Q.; Tiefenbacher, K. Hexameric Resorcinarene Capsule is a Brønsted Acid: Investigation and Application to Synthesis and Catalysis. *J. Am. Chem. Soc.* **2013**, *135* (43), 16213−16219.
(40) Gaeta, C.; Talotta, C.; De Rosa, M.; La Manna, P.; Soriente, A.; Neri, P. The Hexameric Resorcinarene Capsule at Work: Supramolecular Catalysis in Confined Spaces. *Chem. - Eur. J.* **2019**, *25*, 4899−4913.
(41) Gambaro, S.; Talotta, C.; Sala, P. D.; Soriente, A.; De Rosa, M.; Gaeta, C.; Neri, P. Kinetic and Thermodynamic Modulation of Dynamic Imine Libraries Driven by the Hexameric Resorcinarene Capsule. *J. Am. Chem. Soc.* **2020**, *142* (35), 14914−14923.
(42) Gambaro, S.; La Manna, P.; De Rosa, M.; Soriente, A.; Talotta, C.; Gaeta, C.; Neri, P. The Hexameric Resorcinarene Capsule as a Brønsted Acid Catalyst for the Synthesis of Bis(heteroaryl)methanes in a Nanoconfined Space. *Front. Chem.* **2019**, *7*, 687.
(43) La Sorella, G.; Sperni, L.; Strukul, G.; Scarso, A. Supramolecular Activation of Hydrogen Peroxide in the Selective Sulfoxidation of Thioethers by a Self-Assembled Hexameric Capsule. *Adv. Synth. Catal.* **2016**, *358*, 3443−3449.
(44) La Sorella, G.; Sperni, L.; Strukul, G.; Scarso, A. Supramolecular Encapsulation of Neutral Diazoacetate Esters and Catalyzed 1,3-Dipolar Cycloaddition Reaction by a Self-Assembled Hexameric Capsule. *ChemCatChem* **2015**, *7* (2), 291−296.
(45) Giust, S.; La Sorella, G.; Sperni, L.; Fabris, F.; Strukul, G.; Scarso, A. Supramolecular Catalysis in the Synthesis of Substituted 1 H-Tetrazoles from Isonitriles by a Self-Assembled Hexameric Capsule. *Asian J. Org. Chem.* **2015**, *4* (3), 217−220.
(46) Gambaro, S.; De Rosa, M.; Soriente, A.; Talotta, C.; Floresta, G.; Rescifina, A.; Gaeta, C.; Neri, P. A hexameric resorcinarene capsule as a hydrogen bonding catalyst in the conjugate addition of pyrroles and indoles to nitroalkenes. *Org. Chem. Front.* **2019**, *6*, 2339−2347.
(47) La Manna, P.; De Rosa, M.; Talotta, C.; Rescifina, A.; Floresta, G.; Soriente, A.; Gaeta, C.; Neri, P. Synergic Interplay Between Halogen Bonding and Hydrogen Bonding in the Activation of a Neutral Substrate in a Nanoconfined Space. *Angew. Chem., Int. Ed.* **2020**, *59* (2), 811−818.
(48) Giust, S.; La Sorella, G.; Sperni, L.; Fabris, F.; Strukul, G.; Scarso, A. Supramolecular Catalysis in the Synthesis of Substituted 1 H-Tetrazoles from Isonitriles by a Self-Assembled Hexameric Capsule. *Asian J. Org. Chem.* **2015**, *4* (3), 217−220.
(49) Köster, J. M.; Häussinger, D.; Tiefenbacher, K. Activation of Primary and Secondary Benzylic and Tertiary Alkyl (sp^3)C-F Bonds Inside a Self-Assembled Molecular Container. *Front. Chem.* **2019**, *6*, 639.
(50) La Manna, P.; De Rosa, M.; Talotta, C.; Gaeta, C.; Soriente, A.; Floresta, G.; Rescifina, A.; Neri, P. The hexameric resorcinarene capsule as an artificial enzyme: ruling the regio and stereochemistry of a 1,3-dipolar cycloaddition between nitrones and unsaturated aldehydes. *Org. Chem. Front.* **2018**, *5*, 827−837.
(51) La Manna, P.; Talotta, C.; Floresta, G.; De Rosa, M.; Soriente, A.; Rescifina, A.; Gaeta, C.; Neri, P. Mild Friedel−Crafts Reactions inside a Hexameric Resorcinarene Capsule: C−Cl Bond Activation through Hydrogen Bonding to Bridging Water Molecules. *Angew. Chem., Int. Ed.* **2018**, *57*, 5423−5428.
(52) Catti, L.; Zhang, Q.; Tiefenbacher, K. Advantages of Catalysis in Self-Assembled Molecular Capsules. *Chem. - Eur. J.* **2016**, *22*, 9060−9066.
(53) Köster, J. M.; Tiefenbacher, K. Elucidating the Importance of Hydrochloric Acid as a Cocatalyst for Resorcinarene-Capsule-Catalyzed Reactions. *ChemCatChem* **2018**, *10*, 2941−2944.
(54) La Sorella, G.; Sperni, L.; Ballester, P.; Strukul, G.; Scarso, A. Hydration of aromatic alkynes catalyzed by a self-assembled hexameric organic capsule. *Catal. Sci. Technol.* **2016**, *6*, 6031−6036.
(55) Catti, L.; Zhang, Q.; Tiefenbacher, K. Self-Assembled Supramolecular Structures as Catalysts for Reactions Involving Cationic Transition States. *Synthesis* **2016**, *48*, 313−328.
(56) Zhang, Q.; Catti, L.; Kaila, V. R. I.; Tiefenbacher, K. To catalyze or not to catalyze: elucidation of the subtle differences between the hexameric capsules of pyrogallolarene and resorcinarene. *J. Am. Chem. Sci.* **2017**, *8* (2), 1653−1657.
(57) Levi, S.; Zhang, Q.; Major, D. T. Thermodynamic and Kinetic Control Determine the Sesquiterpene Reaction Pathways Inside Nanocapsules. *ACS Catal.* **2020**, *10* (12), 6843−6853.
(58) Zhang, Q.; Catti, L.; Pleiss, J.; Tiefenbacher, K. Terpene Cyclizations inside a Supramolecular Catalyst: Leaving-Group-Controlled Product Selectivity and Mechanistic Studies. *J. Am. Chem. Soc.* **2017**, *139* (33), 11482−11492.
(59) Zhu, Y.; Rebek, J., Jr.; Yu, Y. Cyclizations catalyzed inside a hexameric resorcinarene capsule. *Chem. Commun.* **2019**, *55*, 3573−3577.
(60) Merget, S.; Catti, L.; Piccini, G.; Tiefenbacher, K. Requirements for Terpene Cyclizations inside the Supramolecular Resorcinarene Capsule: Bound Water and Its Protonation Determine the Catalytic Activity. *J. Am. Chem. Soc.* **2020**, *142* (9), 4400−4410.
(61) Zhang, Q.; Rinkel, J.; Goldfuss, B.; Dickschat, J. S.; Tiefenbacher, K. Sesquiterpene cyclizations catalysed inside the resorcinarene capsule and application in the short synthesis of isolongifolene and isolongifolenone. *Nat. Catal.* **2018**, *1* (8), 609−615.
(62) Syntrivanis, L. D.; Némethová, I.; Schmid, D.; Levi, S.; Prescimone, A.; Bissegger, F.; Major, D.; Tiefenbacher, K. Four-Step Access to the Sesquiterpene Natural Product Presilphiperfolan-1β-ol and Unnatural Derivatives via Supramolecular Catalysis. *J. Am. Chem. Soc.* **2020**, *142*, 5894−5900.
(63) Zhang, Q.; Tiefenbacher, K. Sesquiterpene Cyclizations inside the Hexameric Resorcinarene Capsule: Total Synthesis of δ-Selinene and Mechanistic Studies. *Angew. Chem., Int. Ed.* **2019**, *58* (36), 12688−12695.
(64) Shimizu, S.; Usui, A.; Sugai, M.; Suematsu, Y.; Shirakawa, S.; Ichikawa, H. Hexameric Capsule of a Resorcinarene Bearing Fluorous Feet as a Self-Assembled Nanoreactor: A Diels−Alder Reaction in a Fluorous Biphasic System. *Eur. J. Org. Chem.* **2013**, *22*, 4734−4737.
(65) Jans, A. C. H.; Caumes, X.; Reek, J. N. H. Gold Catalysis in (Supra)Molecular Cages to Control Reactivity and Selectivity. *ChemCatChem* **2018**, *10*, 1−12.
(66) Cavarzan, A.; Reek, J. N. H.; Trentin, F.; Scarso, A.; Strukul, G. Substrate selectivity in the alkyne hydration mediated by NHC−Au(i) controlled by encapsulation of the catalyst within a hydrogen bonded hexameric host. *Catal. Sci. Technol.* **2013**, *3*, 2898−2901.
(67) Jans, A. C. H.; Gómez-Suárez, A.; Nolan, S. P.; Reek, J. N. H. A Switchable Gold Catalyst by Encapsulation in a Self-Assembled Cage. *Chem. - Eur. J.* **2016**, *22* (42), 14836−14839.
(68) Jongkind, L. J.; Rahimi, M.; Poole, D.; Ton, S. J.; Fogg, D. E.; Reek, J. N. H. Protection of Ruthenium Olefin Metathesis Catalysts by Encapsulation in a Self-assembled Resorcinarene Capsule. *ChemCatChem* **2020**, *12*, 4019−4023.
(69) Zhang, Q.; Catti, L.; Tiefenbacher, K. Catalysis inside the Hexameric Resorcinarene Capsule. *Acc. Chem. Res.* **2018**, *51*, 2107−2114.
(70) Bräuer, T. M.; Zhang, Q.; Tiefenbacher, K. Iminium Catalysis inside a Self-Assembled Supramolecular Capsule: Modulation of Enantiomeric Excess. *Angew. Chem., Int. Ed.* **2016**, *55*, 7698−7701.
(71) Bräuer, T. M.; Zhang, Q.; Tiefenbacher, K. Iminium Catalysis inside a Self-Assembled Supramolecular Capsule: Scope and Mechanistic Studies. *J. Am. Chem. Soc.* **2017**, *139* (48), 17500−17507.
(72) Payne, R. M.; Oliver, C. L. A propanol-seamed C-methylcalix[4]-resorcinarene hexamer accessible via solution crystallization, liquid-assisted grinding and vapour sorption. *CrystEngComm* **2018**, *20* (14), 1919−1922.
(73) Avram, L.; Cohen, Y. The Role of Water Molecules in a Resorcinarene Capsule As Probed by NMR Diffusion Measurements. *Org. Lett.* **2002**, *4* (24), 4365−4368.
(74) Slovak, S.; Avram, L.; Cohen, Y. Encapsulated or Not Encapsulated? Mapping Alcohol Sites in Hexameric Capsules of Resorcin[4]arenes in Solution by Diffusion NMR Spectroscopy. *Angew. Chem., Int. Ed.* **2010**, *49* (2), 428−431.

https://doi.org/10.1021/jacs.1c04924
J. Am. Chem. Soc. 2021, 143, 16419−16427

(75) Slovak, S.; Cohen, Y. The Effect of Alcohol Structures on the Interaction Mode with the Hexameric Capsule of Resorcin[4]arene. *Chem. - Eur. J.* **2012**, *18*, 8515−8520.
(76) Schnatwinkel, B.; Stoll, I.; Mix, A.; Rekharsky, M. V.; Borovkov, V. V.; Inoue, Y.; Mattay, J. Monomeric, dimeric and hexameric resorcin[4]arene assemblies with alcohols in apolar solvents. *Chem. Commun.* **2008**, No. 33, 3873−3875.
(77) Katiyar, A.; Freire Sovierzoski, J. C.; Calio, P. B.; Vartia, A. A.; Thompson, W. H. Water plays a diverse role in a hydrogen-bonded, hexameric supramolecular assembly. *Chem. Commun.* **2019**, *55* (46), 6591−6594.
(78) Katiyar, A.; Freire Sovierzoski, J. C.; Calio, P. B.; Vartia, A. A.; Thompson, W. H. Water plays a dynamical role in a hydrogen-bonded, hexameric supramolecular assembly. *Phys. Chem. Chem. Phys.* **2020**, *22*, 6167−6175.
(79) Ramsey, S.; Nguyen, C.; Salomon-Ferrer, R.; Walker, R. C.; Gilson, M. K.; Kurtzman, T. Solvation thermodynamic mapping of molecular surfaces in AmberTools: GIST. *J. Comput. Chem.* **2016**, *37* (21), 2029−2037.
(80) Bryant, R. G. The NMR time scale. *J. Chem. Educ.* **1983**, *60* (11), 933−935.
(81) Fulmer, G. R.; Miller, A. J. M.; Sherden, N. H.; Gottlieb, H. E.; Nudelman, A.; Stoltz, B. M.; Bercaw, J. E.; Goldberg, K. I. NMR Chemical Shifts of Trace Impurities: Common Laboratory Solvents, Organics, and Gases in Deuterated Solvents Relevant to the Organometallic Chemist. *Organometallics* **2010**, *29*, 2176−2179.
(82) Ouellette, R. J. the Chemical Shift of the Hydroxyl Proton of Phenols in Dimethyl Sulfoxide. *Can. J. Chem.* **1965**, *43*, 707−709.
(83) Beckett, M. A.; Strickland, G. C.; Holland, J. R.; Sukumar Varma, K. A convenient n.m.r. method for the measurement of Lewis acidity at boron centres: correlation of reaction rates of Lewis acid initiated epoxide polymerizations with Lewis acidity. *Polymer* **1996**, *37* (20), 4629−4631.
(84) Mayer, U.; Gutmann, V.; Gerger, W. The acceptor number: A quantitative empirical parameter for the electrophilic properties of solvents. *Monatsh. Chem.* **1975**, *106* (6), 1235−1257.
(85) Oka, K.; Shibue, T.; Sugimura, N.; Watabe, Y.; Winther-Jensen, B.; Nishide, H. Long-lived water clusters in hydrophobic solvents investigated by standard NMR techniques. *Sci. Rep.* **2019**, *9* (1), 1−6.
(86) Jakubczyk, M.; Adamczyk-Woźniak, A.; Sporzyński, A. Acceptor number of organoboron molecules quantitative determination of Lewis acidity. In *Molecular Receptors.*; East Publisher House, 2011. pp 53−68.

https://doi.org/10.1021/jacs.1c04924
J. Am. Chem. Soc. 2021, 143, 16419−16427